Wet-GC: A Novel Multimodel Graph Convolutional Approach for Wetland Classification Using Sentinel-1 and 2 Imagery With Limited Training Samples

Hamid Jafarzadeh, *Student Member, IEEE*, Masoud Mahdianpari, *Senior Member, IEEE*, and Eric W. Gill, *Senior Member, IEEE*

***Abstract*—Wetland is one of the most productive resources on earth, and it provides vital habitats for several unique species of flora and fauna. Over the last decade, mapping and monitoring wetlands by utilizing deep learning (DL) models and remote sensing data gained popularity due to the importance of wetland preservation. In general, DL-based methods have shown astonishing achievement in wetland classification, but some practical issues, such as limited training samples, still need to be addressed. Moreover, the performance of most of the DL approaches is decreased when moderate-resolution images with few features are used as input data. One solution to breaking the performance bottleneck of a single model is to fuse two or more of them. To this end, we strive to investigate and develop a multimodel DL algorithm for wetland classification based on the combination of a graph convolutional network (GCN) and a shallow convolutional neural network (CNN), which is called the Wet-GC algorithm hereinafter. In doing this, moderate-resolution Sentinel-1 (S1) synthetic aperture radar (SAR) and Sentinel-2 (S2) multispectral optical imagery are fed into the GCN and CNN models, respectively. As we know from the literature, the synergistic use of S1 SAR and S2 optical imagery can be used to extract different types of wetland features and increase the class discrimination possibility. Hence, wetland mapping by jointly using GCN and CNN has the ability to boost the wetland classification task. Findings indicate that the efficiency of Wet-GC with an overall accuracy (OA) of 88.68% outperforms the results obtained from random forest (OA = 84.88%), support vector machine (OA = 82.86%), extreme gradient boosting (OA = 86.55%), and ResNet50 (OA = 86.93%). The outcomes reveal that the Wet-GC architecture proposed in this article has an excellent capability to be applied over large areas with minimal need for training samples and can perform acceptably in supporting regional wetland mapping.**

***Index Terms*—Canada, classification, convolutional neural network (CNN), deep learning (DL), graph convolutional network (GCN), remote sensing (RS), sentinel, wetlands.**

Manuscript received 3 March 2022; revised 23 April 2022; accepted 6 May 2022. Date of publication 22 June 2022; date of current version 13 July 2022. The work of Masoud Mahdianpari was supported by the Natural Sciences and Engineering Research Council (NSERC) Discovery under Grant RGPIN-2022-04766. The work of Eric W. Gill was supported by the NSERC Discovery under Grant RGPIN-2020-05003. *(Corresponding author: Masoud Mahdianpari.)*

Hamid Jafarzadeh and Eric W. Gill are with the Department of Electrical and Computer Engineering, Memorial University of Newfoundland, St. John's, NL A1B 3X5, Canada (e-mail: hjafarzadeh@mun.ca; ewgill@mun.ca).

Masoud Mahdianpari is with the Department of Electrical and Computer Engineering, Memorial University of Newfoundland, St. John's, NL A1B 3X5, Canada, and also with the C-CORE, St. John's, NL A1B 3X5, Canada (e-mail: m.mahdianpari@mun.ca).

Digital Object Identifier 10.1109/JSTARS.2022.3177579

I. Introduction

WETLANDS are most simply defined as areas that are at least periodically covered by or saturated with water and include active plants during each year's growing season and water saturation period [1]–[5]. Wetlands are some of the most productive resources on earth and support a host of ecosystem services [1], [4], [6], [7]. In particular, they provide innumerable functions, such as natural drinking water filtration, flood and drought relief, shoreline erosion protection, soil conservation, biodiversity preservation, and carbon sequestration, to name a few [3], [6], [8]–[10]. Wetlands also have an impact on climate change in that they help regulate regional climate [4], [11]. As such, these considerations confirm that wetlands can provide huge economical, ecological, cultural, recreational, and aesthetical worldwide benefits [12]–[14]. In spite of these positive impacts, due to human disturbance, wetlands have been polluted and drained severely over the past five decades as some regions' land covers have changed (e.g., wetlands conversion to urban or agricultural land use) [1], [3]. The loss in wetlands areas has severe impacts on the valuable services they provide for humans and nonhumans alike [3], [7], [15]. Therefore, improving the requirements for wetland studies and monitoring the status of wetlands is essential for maintaining such vital features of the landscape.

Remote sensing (RS) is the foremost source of spatial and temporal information about earth's surface constitution [16]. Despite several advances in RS technology, certain factors make wetlands challenging to map through satellite imagery [17]. Of these factors, the main ones are 1) ecological similarities of wetland classes with each other (among types of wetlands are bog, fen, marsh, and swamp, as outlined and explained by the Canadian Wetland Classification System [18]) and also with other nonwetland classes (e.g., water, forest, agriculture, …) [19]–[21]; and 2) highly dynamic characteristics of wetland classes that substantially alter their reflectance and energy backscatter properties, especially within a growing season [22], [23]. However, these challenges can be overcome by selecting appropriate machine learning (ML) algorithms.

Given the need for up-to-date landscape information, along with broad-scale coverage of wetland areas (i.e., regional, national, and global context), satellite RS plays the main role as an efficient and cost-effective method in such a vital task [24], [25].

Different sensors in RS, however, capture a wide range of earth surface information from different perspectives. Within the RS community, a particularly interesting challenge is how to effectively combine multiple complementary data sources. Previous studies highlight improvements in the performance of a variety of RS-based applications by integrating multisource/multisensor RS data. For instance, by using multisource moderate resolution RS data, Shen *et al.* [26] applied deep learning (DL) technique to predict the main factors for drought monitoring. In [27], a multiple-layers DL architecture was designed for change detection with multisource VHR satellite images. Li *et al.* [28] proposed a DL network to extract water bodies based on multisource RS data. The use of integrated features of multisource datasets has also contributed to the classification of wetland areas [29].

Specifically, optical and synthetic aperture radar (SAR) sensors are based on range and angular measurements and collect information about wetland vegetation's chemical and physical characteristics, respectively [8]. The combination of optical and SAR images has a number of advantages and can be applied to improve the wetland mapping, thanks to the complementary information provided by both sources. The optical sensors obtain information from the reflection and emission characteristics of the earth's surface, while the SAR sensors provide information based on the structural and dielectric properties of natural and man-made objects [30]. So, a feature that is not visible in the optical images may be visible in the SAR data (and vice versa), and using only the optical images can lead to misclassification. The inclusion of SAR data can avoid this distinction, as features with similar spectral characteristics may have different distribution patterns in the SAR images. Therefore, incorporating both optical and SAR datasets adds more information on wetlands and consequently enhances the discrimination of different wetland types [31]–[33].

Fortunately, through the development of innovative models, numerous studies in the literature have attempted to deal with wetland classification challenges with a minimal need for *in situ* measurements. However, for the following reasons, most models related to large-scale scattering are not very effective in wetland classification.

1) Current large-scale satellite imagery does not use high spatial and spectral resolution sensors, and this imposes challenges in distinguishing classes exclusively by analyzing their spectra.
2) Cost and accessibility issues associated with some kinds of satellite images (e.g., high-resolution and hyperspectral data) prevent the utilization of several approaches in practice [34], [35].
3) A large amount of *in situ* measurements are not available for large-scale and inaccessible wetland areas, and since the efficiency of DL methods significantly depends on the availability of a large number of training samples, not every methodology is executable.
4) Wetland classes have considerable internal variability caused by the large spatial coverage of satellite retrieved data; thus, the class separability in a restricted neighborhood is a complex problem.

Considering the points raised previously, proposing a proper ML algorithm and utilizing available free-of-charge satellite imagery is still needed in order to make a significant contribution to wetland mapping.

To date, several DL approaches have been developed for diverse kinds of RS images, from coarse resolution to high-resolution satellite imagery and from multispectral to hyperspectral datasets with hundreds of bands. Owing to the impressive feature representation power of the convolutional neural network (CNN), it has been employed in a broad scope of RS applications such as image classification [36], [37], change detection [38], and semantic segmentation [39]. For classification purposes, for instance, Wang *et al.* [40] introduced a deep feature learning-based method to improve scene classification by incorporating rich hierarchical features of a CNN model. Liu *et al.* [41] proposed a scene classification approach based on Siamese CNN, which combines verification and identification models to boost performance. These two models are used to predict the input images' identity labels and measure the similarities between image pairs, respectively. To support arbitrary sizes of the input images without any resizing process, Xie *et al.* [42] designed a scale-free CNN to prevent information discard in high spatial resolution images and improve scene classification performance.

Several attempts have been made to use DL models for wetland classification in the last few years. For instance, in [43], a pretrained AlexNet model was applied to the RapidEye multispectral dataset to classify complex wetland land cover. Its results were compared with those of the random forest model. DeLancey *et al.* used optical and SAR images to investigate the effectiveness of deep CNN on large-scale wetland classification. They reported the successful discriminability of the wetland categories using CNN models [21]. Furthermore, in [44], an encoder–decoder CNN model was proposed to classify wetland classes using LiDAR and spectral indices as input. To provide an spatio-temporal architecture, Hosseiny *et al.* established a workflow named WetNet for wetland mapping considering 2D-CNN, 3D-CNN, and LSTM layers. The efficiency of their model was evaluated utilizing S1 and S2 images [29]. In a recent publication, Jamali and Mahdianpari [45] focused on the integration of CNN models with transformers and suggested a multimodel DL network for wetland classification by the integration of a modified version of VGG-16, a 3D-CNN, and the Swin transformer.

Benefiting from the fast development of DL approaches, the progress in RS image classification has been accelerated. Several graph convolutional network (GCN) based methods have recently been proposed in the RS community. These studies have investigated the potential of such a powerful model for RS scene classification using optical data [46], [47]. In [48], a graph attention network, which is a modification of GCN, was suggested for hyperspectral image classification. To exploit the spatial information of a hyperspectral image as well as its spectral information, context-aware GCN, and multiscale GCN algorithms were established in [49] and [50], respectively. In addition, a nonlocal GCN, which took the whole hyperspectral image as input to learning graph representations, was explored in [51].

Given that the traditional GCN model utilizes the adjacency matrix, it suffers from a high computational cost, particularly in large-scale RS problems. To solve this issue, very recently, Hong *et al.* [52] proposed a minibatch GCN framework for hyperspectral image classification. Instead of feeding all the data into the network at once, this method proceeds in several batches, reducing the computational cost compared to the traditional GCN model. Despite the effectiveness of the GCN structure, there is no documented research on the application of this powerful model either for wetland classification or the combination of SAR and optical imagery. The literature review indicates that GCNs have not been widely applied to commonly used free publicly available satellite imagery (e.g., Sentinel and Landsat images) compared to hyperspectral data. Since these publicly available moderate-resolution datasets (e.g., 10–30 m) are extensively used in both RS-based academic and practical fields, there needs to be more research on the potential of GCNs on such imagery.

With the current status of DL algorithms employed in wetland mapping in mind, we will propose a new classification framework that combines GCNs and CNNs utilizing moderate-resolution S1 and S2 satellite imagery. The focus of this article lies in the prediction of wetland classes. Here, we summarize the contributions of this article in addressing the issues of large-scale wetland landscape classification through RS imagery and provide a framework to reach better results. In order to make the synergistic use of the S1 and S2 datasets, the proposed framework (i.e., Wet-GC) is devised in two branches as follows.

1) The GCN branch: The GCN architecture will be introduced first, focusing on incorporating the spatial context of images in wetland classification as the spectral context. As verified, this framework is able to produce good results in the classification of hyperspectral benchmark datasets. To our knowledge, this article is the first one that modifies and employs such a potentially effective network for wetland classification.
2) The CNN branch: A simple shallow CNN architecture will also be introduced and added to the model as the second branch.

The main objective for creating a two-branch Wet-GC network in this article is to take advantage of each branch's unique capabilities when dealing with multisource data. The optical imagery contains rich spectral information that offers an opportunity to study land covers. Studies using DL have demonstrated that CNNs can learn image features automatically by collecting spectral contextual information from multispectral images. As a result, CNNs are frequently cited in the literature as effective models for classifying land covers using S2 optical data [53], [54]. As such, S2 is the input of the CNN branch of the proposed Wet-GC. With less contextual information available in SAR data, the CNN branch is inefficient for exploring S1 imagery, as frequently reported in the literature. Therefore, the Wet-GC approach employs a GCN branch to establish the directional associations between pixels in S1 SAR data. In comparison to the CNN branch, the GCN branch is more capable of polarimetric information extraction in SAR data. Thus, SAR data have been considered as input in the GCN branch of the proposed Wet-GC network.

In Section II, the basic preliminaries of GCN are presented. The details of Wet-GC architecture are introduced in Section III. Section IV contains an introduction of the study area, datasets, and the experimental setup utilized in this article. Discussion of the results appears in Section VI. Finally, Section V concludes this article.

II. Related Work

This section provides basic preliminaries of GCN and mini-GCN and the related equations. First, consideration is given as to what a "graph" is. Subsequently, we will discuss constructing the adjacency matrix and using it with Fourier transform equations to express the convolution operation on a graph.

The neural network concept for directly processing graph data was first introduced in [55]. In the case of RS data analysis, a graph is explained as the relations of spectral/ backscattering signatures in an image domain. A graph $\mathcal{G}$ is defined by two components: $\mathcal{G} = (\mathcal{V}, \mathcal{E})$ in which $\mathcal{V}$ denotes the vertices (i.e., the pixel vectors in the image domain) and $\mathcal{E}$ denotes the edges (i.e., the similarities between the two $\mathcal{V}_i$ and $\mathcal{V}_j$ vertices) [52]. This similarity is defined by an adjacency matrix denoted as A, which is computed using the radial basis function (RBF) for any two x_i and x_j spectral signatures associated with the vertices $\mathcal{V}_i$ and $\mathcal{V}_j$ as given by

$$A_{i,j} = exp\left(-\frac{x_i - x_j^2}{\sigma^2}\right) \tag{1}$$

where the value for the σ parameter controls the width of the RBF. By knowing both the adjacency matrix (A) and the matrix trace of A (sum of diagonal elements of the matrix A, i.e., $D_{i,i} = \sum_j A_{i.j}$ [52], [56]), the Laplacian matrix L and the symmetric normalized Laplacian matrix (L_{sym}) can be computed as

$$L = D - A \tag{2}$$

$$L_{sym} = D^{-\frac{1}{2}} L D^{-\frac{1}{2}} = I - D^{-\frac{1}{2}} A D^{-\frac{1}{2}}. \tag{3}$$

In mathematics and, in particular, functional analysis, the "Convolution" is an operation involving two functions by the integral of the pointwise multiplication of those functions. Let us now discuss shortly on graph convolutions and their related equations in the spectral domain. Through the practical Fourier and inverse Fourier transforms [52], [57], the convolution theorem of the given two functions f and g can be expressed as

$$f(t) \otimes g(t) = \mathcal{F}^{-1} \{\mathcal{F}[f(t)] . \mathcal{F}[g(t)]\} \tag{4}$$

where "$\otimes$" denotes the convolution operation.

According to (4), the convolution operation on a graph can be expressed in terms of the Fourier transform ($\mathcal{F}$) and subsequently as a series of basis functions. In other words, as proven in [52], the eigenvectors of L, i.e., $\mathrm{U} = (u_1, u_2, \ldots, u_n)$ are the same as the basis functions of $\mathcal{F}$ and is expressed as

$$L = U \Lambda U^{-1} \tag{5}$$

and since U is an orthogonal matrix, i.e., its transpose (U^{T}) is equal to its inverse matrix (U^{-1}), then (5) can be written as

$$L = U \Lambda U^{-1} = U \Lambda U^{T} \tag{6}$$

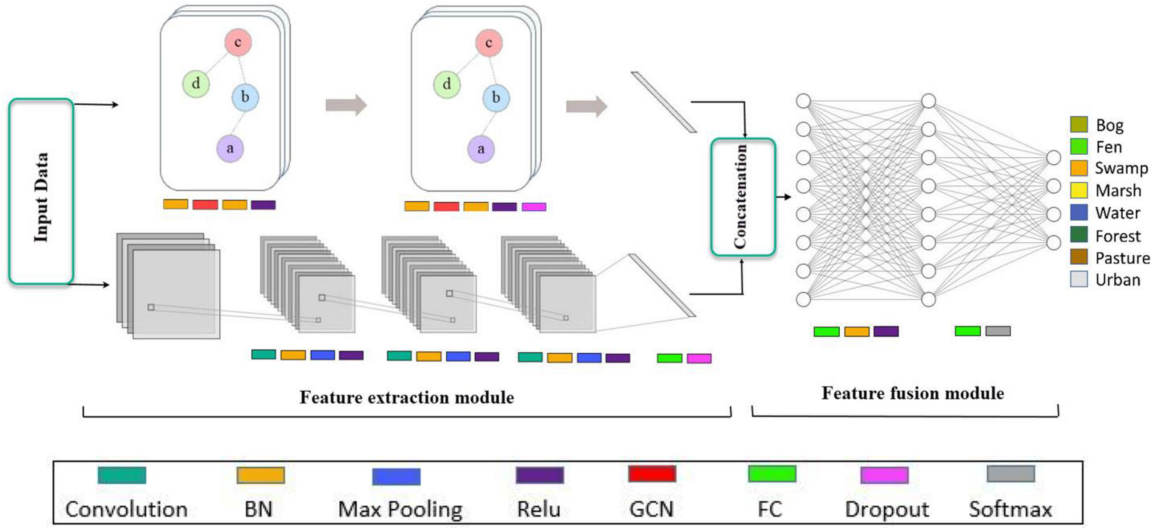

Fig. 1. General flowchart of the proposed Wet-GC model. The feature extraction module extracts different features by using both CNNs and GCNs. The feature fusion module concatenates the resulting features as the final classification input.

where Λ is a diagonal matrix of L's eigenvalues. So that considering (6), the Fourier transform and the inverse Fourier transform of function f on a graph is identical to

$$\mathcal{GF}\ [f] = U^T\ f \tag{7}$$

$$f = U\mathcal{GF}\,[f]\,. \tag{8}$$

Therefore, (4) can be converted to

$$\mathcal{G}\ [f \otimes g] = U\left\{\left[U^T f\right].\left[U^T g\right]\right\}. \tag{9}$$

If we write $U^T g$ as g_θ and consider doing some computational complexity simplification, the convolution on a graph can be formulated as

$$\mathcal{G}\,[f \otimes g_\theta] \approx \theta\left(I + D^{-\frac{1}{2}} A D^{-\frac{1}{2}}\right) f. \tag{10}$$

Finally, by using (10), the propagation rule for GCNs will be as follows:

$$H^{(\ell+1)} = h\left(\tilde{D}^{-\frac{1}{2}}\tilde{A}\tilde{D}^{-\frac{1}{2}} H^{(\ell)} W^{(\ell)} + b^{(\ell)}\right)$$

$$\tilde{A} = A + I, \quad \text{and} \quad \tilde{D}_{i,i} = \sum_j \tilde{A}_{i,j}\,. \tag{11}$$

Note that $\mathrm{H}^{(\ell)}$ and h are the outputs of ℓth layer and the activation function (with respect to the weights to be learned $\{\mathrm{W}^{(\ell)}\}_{\ell=1}^{P}$ and the biases $\{\mathrm{b}^{(\ell)}\}_{\ell=1}^{P}$ of all layers), respectively [52].

III. Proposed Methodology

The overall architecture of the proposed Wet-GC model is shown in Fig. 1 and is composed of two parts: 1) feature extraction module, including the mini-GCN-based branch and the CNN-based branch; and 2) feature fusion module. The feature extraction module extracts different features by using both CNNs and GCNs. Also, the feature fusion module concatenates the resulted features as the final classification input. These steps will be discussed further in what follows.

TABLE I
Mini-GCN Configuration of the Proposed Wet-GC Framework

Input dimension	D
Sequence	Layer type
Block 1	Batch Normalization GCN Layer Batch Normalization Relu activation function
Block 2	Batch Normalization GCN Layer Batch Normalization Relu activation function Dropout

A. Mini-GCN-Based Branch

GCN is a neural network that learns features by gradually aggregating information in the neighborhood. Fig. 1 and Table I show the architecture of the proposed mini-GCN-based branch. There are some differences between traditional GCNs and mini-GCNs. For the GCNs, all the data usually are used as input at once, which requires a high volume of computations. However, the mini-GCN architecture offers three benefits over the well-known GCNs as follows.

1) It performs a minibatch learning procedure and consequently reduces the computational complexity of the Laplacian matrix and training process and performs fast computations.
2) Minibatch learning acts as a feasible solution to combine the GCN and CNN architectures, and in fact, the mini-GCN procedure makes the GCN trainable in minibatch fashion, analogously to CNN architecture.
3) Minibatch learning also provides spatially local connectivity, which enables the mini-GCN to learn discriminative features from input graph-structured data.

TABLE II
CNN CONFIGURATION OF THE PROPOSED WET-GC FRAMEWORK

Input dimension	$7 \times 7 \times D$	
Sequence	Layer type	Size
Block 1	Convolutional Layer	$(2, 2, 64)$
	Batch Normalization	-
	Max Pooling	(2×2)
	Relu activation function	-
Block 2	Convolutional Layer	$(3, 3, 128)$
	Batch Normalization	-
	Max Pooling	(2×2)
	Relu activation function	-
Block 3	Convolutional Layer	$(3, 3, 256)$
	Batch Normalization	-
	Max Pooling	(2×2)
	Relu activation function	-
Block 4	Fully Connected Layer	-
	Dropout	0.3

Considering (11), the graph convolution in $\mathcal{S}$ batches can be stated as

$$H^{(\ell+1)} = h\left(\tilde{\mathrm{D}}_{\mathcal{S}}^{-\frac{1}{2}}\tilde{\mathrm{A}}_{\mathcal{S}}\tilde{\mathrm{D}}_{\mathcal{S}}^{-\frac{1}{2}}\tilde{\mathrm{H}}_{\mathcal{S}}^{(\ell)}\mathrm{W}^{(\ell)} + \mathrm{b}_{\mathcal{S}}^{(\ell)}\right). \quad (12)$$

In the last equation, $\mathcal{S}$ has reference to both the $\mathcal{S}$th subgraph and batch in the training process of the network. The blocks' sequences utilized for the mini-GCN branch of this article are presented in Table I.

B. CNN-Based Branch

As shown in Fig. 1, the proposed CNN-based branch network has a simple and shallow structure. Generally, CNNs contain three layers: convolutional, pooling, and fully connected (FC) layers. The convolutional layer plays a crucial role in a CNN architecture, and convolution refers to a mathematical operation that merges the input image and filters. This layer includes multiple filters with different sizes that slide across the image grid and learn different portions of input data. In fact, convolution is used for extracting a feature of data by using an arbitrary filter [58], [59]. Typically, after each convolutional layer, a pooling layer is added, which summarizes the features generated in the previous layer and lying within the region covered by the filter, thus, reducing the number of parameters and dimensionality of CNNs [34]. In a standard CNN, the final layer is the FC layer that classifies the features extracted from the last layer into different classes. The structure of the CNN model utilized in this article is presented in Table II.

C. Feature Fusion

There are three well-known and practical strategies, namely additive, elementwise multiplicative, and concatenation, which are used in DL and data processing to combine and fuse the output of different models. For the investigations at hand, as the last step of the Wet-GC architecture, the concatenation strategy is used to fuse/merge the outputs of the mini-GCN and CNN branches to yield a final classification map. In fact, the final output of the proposed framework before entering the classifier is calculated though

$$H_{\text{Total}}^{(\ell+1)} = \left[H_{\text{miniGCNs}}^{(\ell)},\ H_{\text{CNNs}}^{(\ell)}\right]. \quad (13)$$

In order to yield the final output of the Wet-GC network, a FC layer and then a Softmax classifier are applied to the concatenated data. The general overview of the proposed framework for wetland classification is presented in Table III.

TABLE III
GENERAL OVERVIEW OF THE PROPOSED FRAMEWORK FOR WETLAND CLASSIFICATION

Algorithm 1 : The Pseudocode of the Proposed Wet-GC Method for Wetland Classification.

1: $Step1$; {data preparation}
Inputs:
CNN: input S2 data, batchsize
miniGCN: input S1 data, σ value for RBF function
Outputs:
Patches for CNN branch, Laplacian matrix for GCN branch
2: $Step2$; {Jointly using miniGCN and CNN farmework}
Inputs:
number of epochs n for training,
CNN branch: x-train, x-test, y-train, y-test,
miniGCN branch: train-x, train-y, test-x, test-y, Laplacian matrix; minibatch size
LOOP Process:
3: **for** $i = 1$ to n **do**
4: Feature extraction of the lth layer for miniGCN
5: Feature extraction of the lth layer for CNN
6: Calculate the loss
7: Update the weight matrices
8: **end for**
9: Concatenate the outputs of two branches
10: Feature fusion
11: Calculate the network output and conduct label prediction.
Output:
Predict label for input datasets

IV. RESULTS

A. Study Site

Mapping wetlands via RS in Canada is a well-studied topic [19]. The province of Newfoundland is an island located on the eastern-most coast of Canada, and wetlands are a dominant feature of its landscape [3]. In this article, the case study is conducted over part of the Avalon area located in the eastern portion of the province [see Fig. 2(a)].

B. Datasets

1) Field Data: The wetland ground-truth (GT) data that provides the basis for the multiyear reference dataset used in this article was obtained via field campaigns conducted in the summers of 2015 to 2020, initially carried out for use in a project

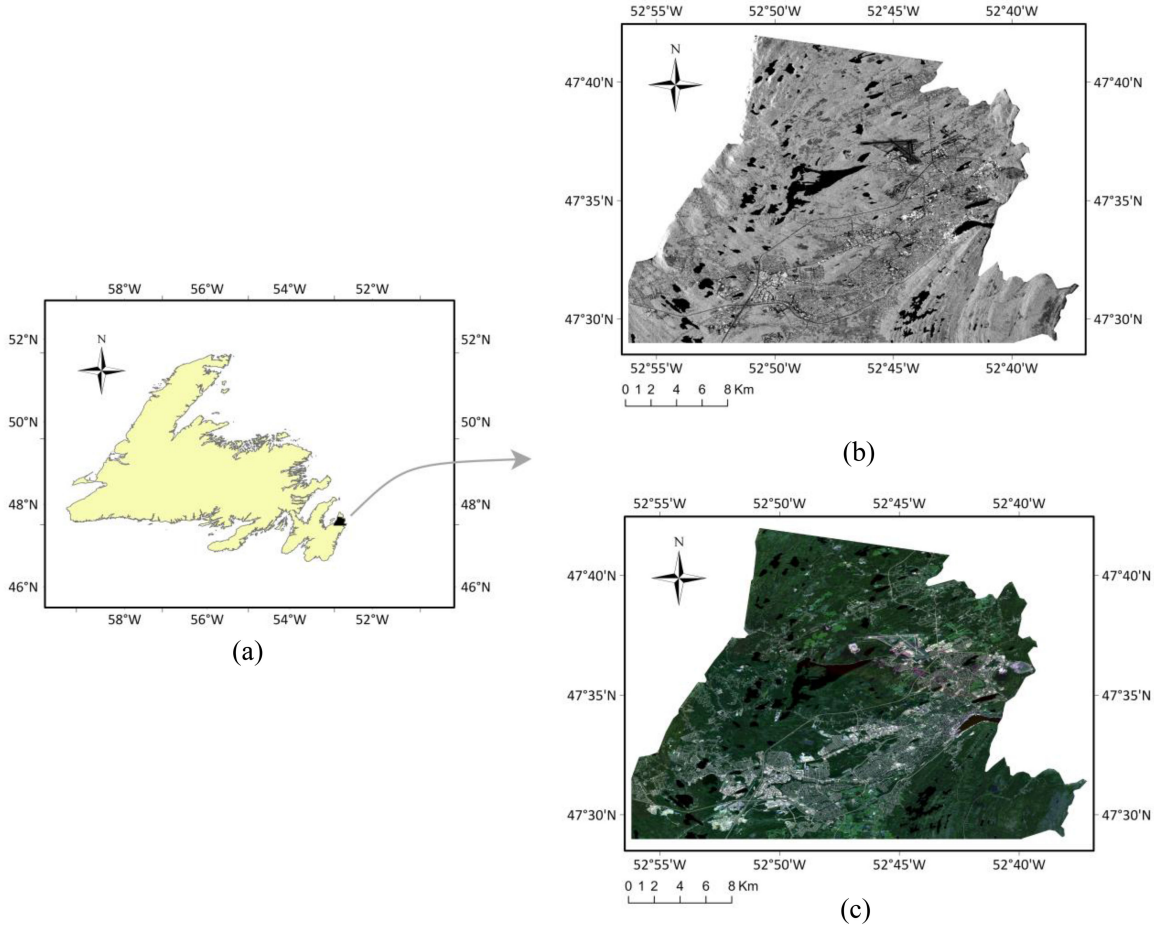

Fig. 2. (a) Location of the study site is in Newfoundland province, Canada. (b) Grayscale VH band illustration of S1 imagery. (c) RGB illustration of S2 imagery.

to develop RS methods for mapping wetlands in Newfoundland and Labrador [3], [60].

2) Sentinel-1 Imagery: The S1 SAR data originated from the Level-1 ground range detected (GRD) interferometric wide swath product as ingested in the cloud-based geospatial processing platform Google Earth Engine (GEE) [61]. This GRD product consisted of S1 radar observations projected onto a regular 10-m grid [62]. The S1 images taken from Jun. 1–Oct. 30, 2020, were selected for this article, and the median reflectance values of the collections were calculated. The primary features recorded by S1 over the case study are the VV and VH polarized backscatter values (in dB). However, the Span and Ratio features (see the formulas in Table IV) were also calculated and stacked to S1 data. A grayscale VH band illustration of S1 imagery from the study area is depicted in Fig. 2(b).

3) Sentinel-2 Imagery: The S2 data are provided in GEE as a Level-1C product representing Top-of-Atmosphere reflectance [63]. A composite based on the median reflectance values of the images taken from Jun. 1–Oct. 30, 2020, with a cloud cover of less than 10% was created. In this article, four bands of S2 image, namely the near-infrared (NIR), red, green, and blue bands, were selected and utilized. These bands have unique characteristics to delineate and discriminate wetland classes. Since water strongly absorbs NIR light, this band was chosen because of its usefulness in distinguishing water content from various land cover types. The Red band has the potential to delineate wetland classes because of its ability to detect chlorophyll absorption in vegetation. Meanwhile, the blue band can reflect the differences between

TABLE IV
BANDS/FEATURES EXTRACTED FROM S1 AND S2 IMAGERY IN THIS ARTICLE

Sensor	Spatial Resolution	Spectral Features	Formula/Symbol
Sentinel-1	10 m	VV	σ^0_{VV}
		VH	σ^0_{VH}
		Span	$\lvert\sigma^0_{VV}\rvert^2 + \lvert\sigma^0_{VH}\rvert^2$
		Ratio	$\lvert\sigma^0_{VV}\rvert^2 \big/ \lvert\sigma^0_{VH}\rvert^2$
Sentinel-2	10 m	*Blue*	*B2*
		Green	*B3*
		Red	*B4*
		NIR	*B8*

σ^0_{XX} and σ^0_{XY} denote co- and cross-polarized sigma nought in the logarithmic scale (dB).

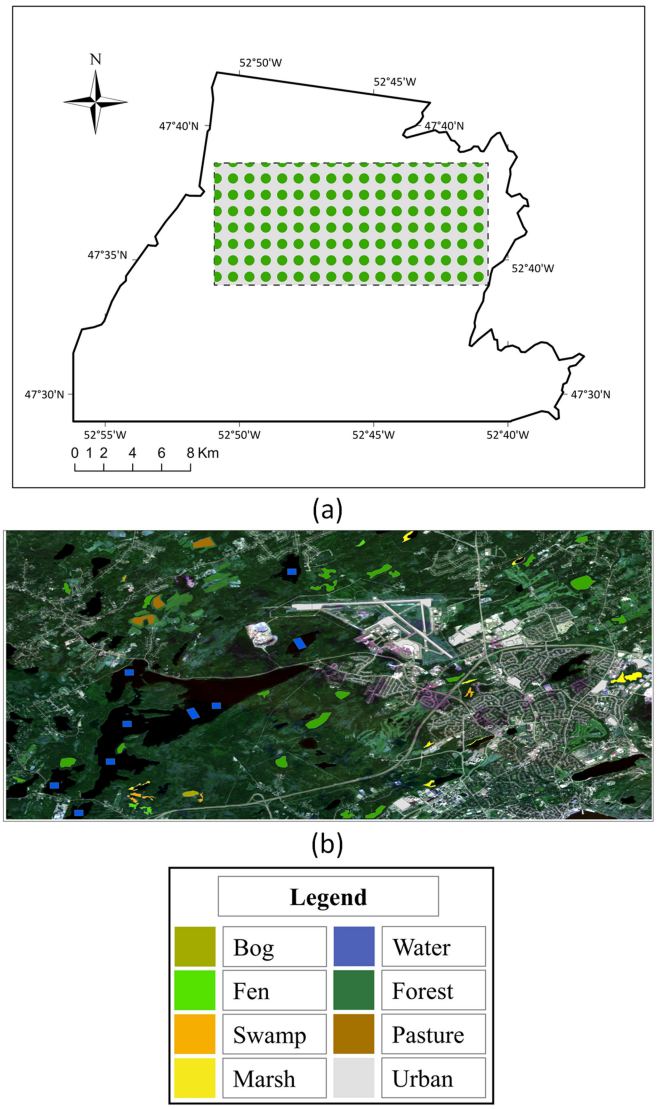

Fig. 3. Snapshot of (a) a portion of the study area in which the reference training samples were selected. (b) Reference wetland and nonwetland data collected in the study area.

soil and vegetation. The green band can act as a valuable input for vegetation extraction as well as being used in a variety of vegetation indices. Excluding the green band may cause some indistinguishably in land covers (e.g., in our case, marsh, and water classes). Moreover, we tried to use only the S2 bands with 10-m spatial resolution (see Table IV). An RGB illustration of S2 imagery from the study area is depicted in Fig. 2(c).

As mentioned earlier, one of the key goals in this article is to develop a novel framework for wetland classification with limited training samples, and this explains the decision to combine GCNs and CNNs. To this end, instead of utilizing all GT data, the training samples are selected just from a portion of the whole study area, as depicted in Fig. 3(a). Note that the chosen area consists of reference data for all kinds of wetland and no-wetland classes mentioned in this article [see Fig. 3(b)]. In addition, the selected GT dataset was randomly split into training and testing samples with a ratio of 10% to 90%, further reducing the training

TABLE V
NUMBER OF SELECTED TRAINING, VALIDATION, AND TESTING PIXELS OF WETLAND CLASSES IN THE STUDY AREA

Class	#Training pixels	#Validation pixels	#Testing pixels	#Pixels in test labels
Bog	584	175	5259	10509
Fen	237	72	2133	4257
Forest	306	92	2750	5500
Marsh	76	25	684	1072
Pasture	509	152	4578	9200
Swamp	69	23	621	1185
Urban	490	147	4403	8828
Water	249	74	2239	4476
Total	2520	760	22669	45027

dataset. The number of training, validation, and testing samples for each category is listed in Table V. Moreover, the number of pixels for the final classification accuracy assessment (number of pixels in test labels) is added to Table V. Note that test labels listed in the last column of this Table were selected from the entire region of the study area to illustrate the generalization capability of the proposed model.

C. Experimental Setup

1) Wetland Classification by Well-Known Models: There are numerous DL and ML models whose robustness has been established in the RS literature. Here, the investigation commences by applying some of these well-known models to S1 and S2 images. Since two different types of satellite datasets are used to investigate the proposed Wet-GC model, in order to maintain the integrity and provide a logical comparison, these datasets are stacked and utilized for the rest of the algorithms employed here. For comparison purposes and to evaluate the efficiency of the Wet-GC, several models, including random forest (RF), support vector machine (SVM), extreme gradient boosting (XGB), and ResNet50 [64] were selected as efficient classifiers for wetland classification, as reported in [29], [34], [65], and [66]. Based on experience reported in [3] and [67], and trial and error, the optimum values for the parameters of RF, SVM, and XGB classifiers are defined and presented in Table VI. All of these models are trained using the limited training samples as explained previously.

2) Wetland Classification by Wet-GC: As noted, the primary purpose of the current research is to develop a novel framework for jointly using mini-GCN and CNN models based on S1 and S2 imagery. To this end, we combined the mini-GCN with a shallow CNN, both of which were discussed earlier. The implementation details of the Wet-GC model are provided in Table VII. Moreover, an ablation experiment (i.e., the accuracy that can be achieved with only a single branch of CNN and GCN models) was also conducted to better understand how each branch of the proposed method improves the wetland classification. The result of this scenario shows an improvement in classification accuracy as compared to several well-known models.

TABLE VI
IMPLEMENTATION DETAILS FOR RF, SVM, AND XGB CLASSIFIERS

Model	Parameter Name	Value
RF	Number of decision trees	150
	Number of variables in each node split	5
	Minimum size of a terminal node	2
	Fraction of the input to bag per tree	0.5
	Number of random seeds	5
SVM	Regularization parameter	3
	Kernel type	RBF
	Degree of the polynomial kernel function	6
XGB	Maximum tree depth	10
	Number of gradient boosted trees	150
	Learning rate	0.1

TABLE VII
IMPLEMENTATION DETAILS FOR THE WET-GC MODEL

Model	Parameter Name	Parameter Value
Wet-GC	Base learning rate	0.0001
	Current learning rate	$\left(1-(Iter/maxIter)\right)^{0.5}$; $Iter = 50$
	Number of epochs	200
	Minibatch size	32
	Dropout	0.3

D. Classification Maps

The classification results of the models implemented here are shown in Fig. 4. Eight distinct land cover classes are depicted on these maps, namely, bog, fen, swamp, marsh, water, forest, pasture, and urban. Furthermore, a zoomed-in representation of a small portion of the classified maps is included in Fig. 5 to investigate and highlight the details of the classification results for different methods.

E. Accuracy Assessment

One of the essential steps in RS applications is to assess the accuracy of the generated products. To this end, several accuracy assessment metrics have been proposed in the literature and applied for different applications. These applications mainly include classification, change detection, and target detection. For the purpose at hand, five metrics, including overall accuracy (OA), recall (sensitivity), specificity, precision, and the F-measure, are used. We refer readers for more information of these metrics to [68]. Moreover, the formulas for the mentioned metrics are presented in Table VIII in which the components "TP," "TN," "FN," and "FP" indicate "True Positive," "True Negative," "False Negative," and "False Positive," respectively.

The quantitative assessment of the classification results of the RF, SVM, XGB, ResNet50, and Wet-GC is shown in Table IX. According to the results, the ResNet50 and XGB models perform better than RF and SVM models. This conclusion seems logical because the robustness of ResNet50 and XGB is also highlighted in comparative evaluation studies, such as appear in [67] and [66]. Although, given the small number of input features (i.e., four features of S1 data and four features of S2 data), it is expected to achieve low accuracy results for RF and SVM models; but the developed Wet-GC architecture has a relatively better performance compared to the other algorithms.

TABLE VIII
ACCURACY ASSESSMENT METRICS

Criteria	Formula
OA	$\frac{(TP+TN)}{(TP+FN+FP+TN)}$
Recall	$\frac{(TP)}{(TP+FN)}$
Specificity	$\frac{(TN)}{(TN+FP)}$
Precision	$\frac{(TP)}{(TP+FP)}$
F-measure	$2\times\frac{Precision\times Recall}{Precision+Recall}$

For further comparison, Fig. 6 shows the confusion matrices of the classification maps. The columns of the confusion matrices denote the classes in the GT data, and the rows show the classes in the predicted maps. It should be noted that each element of the confusion matrices is shown as a percentage calculated from the total number of entries in each column.

F. Computation Run-Time

In order to compare the classification models in terms of computation load, the approximate run-time required for all methods investigated in this article was added to Table X. Although the Wet-GC and ResNet50 models perform well in classification of wetland areas, they have the defect of taking long time to run. The time complexity of the Wet-GC model is due to its two branch architecture and the use of a graph-based structure.

V. DISCUSSION

The quantitative evaluation of results reported in Table IX and Fig. 6 shows that the ResNet50 and XGB methods could correctly detect and classify most classes rather than the RF and SVM. The performance of these models strongly depends on the number of input features and training samples. While the ResNet50 and XGB show better performances, the RF and SVM models failed to provide acceptable results. However, such models do not engender high expectations when using moderate-resolution data with fewer features and limited training samples as input.

Looking at the Wet-GC's result, we find that the classification accuracy has increased relatively. Of the classification results, the Wet-GC method generally produced the highest OA at 88.68%, followed by the ResNet50 at 86.93%, XGB at 86.55%, RF at 84.88%, and SVM at 82.86%. Though the XGB method produced recall and F-score close to that of RF, the RF method had a higher precision (RF precision was 0.6987 compared to 0.6887 XGB precision). In contrast, the XGB method produced a higher specificity compared to RF (Table IX, the XGB specificity was 0.9811, while the RF specificity was 0.9777). Overall, the highest scores of these parameters belong to the

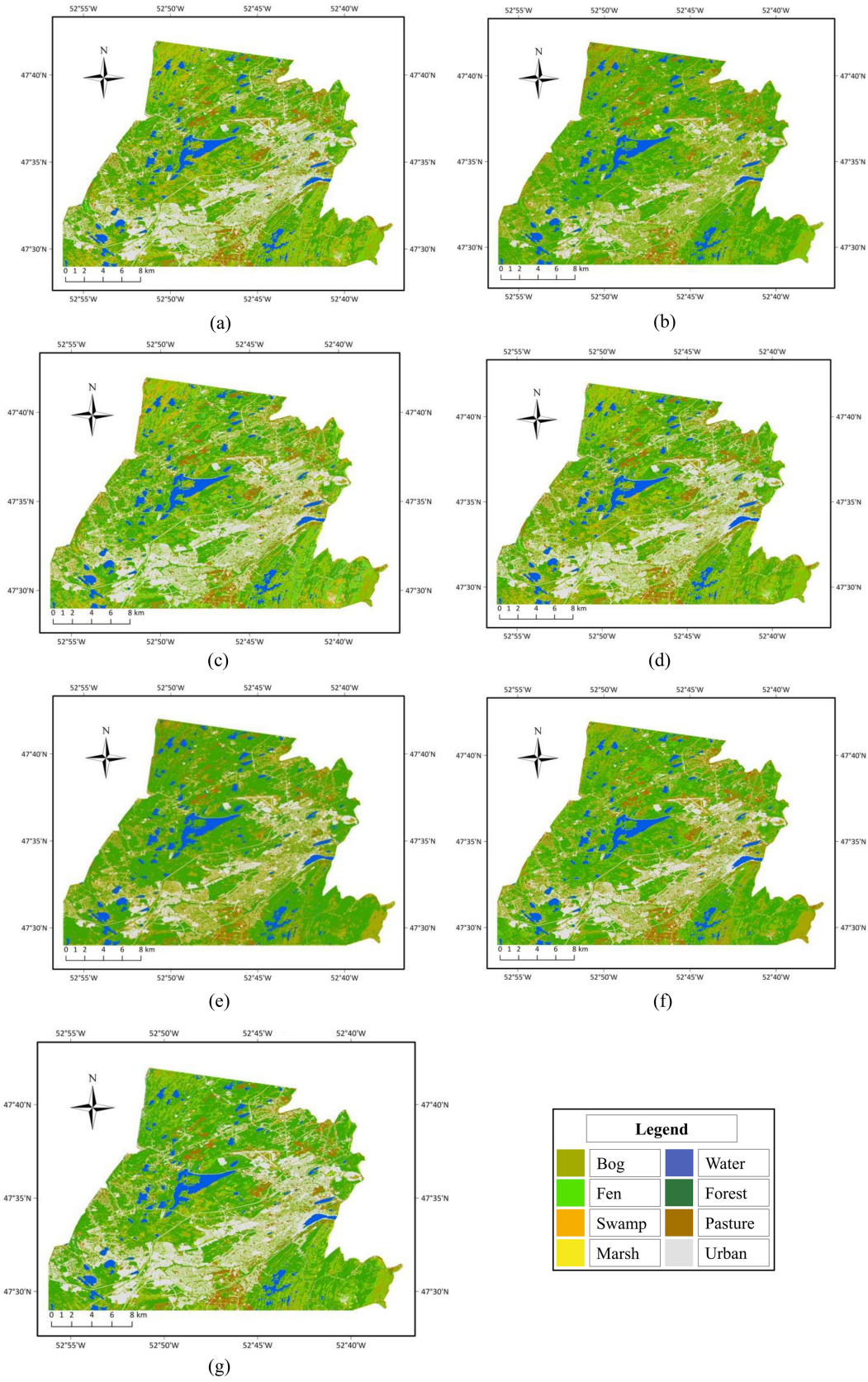

Fig. 4. Resulting classification maps for different methods. (a) RF. (b) SVM. (c) XGB. (d) ResNet50. (e) GCN-branch. (f) CNN-branch. (g) Wet-GC.

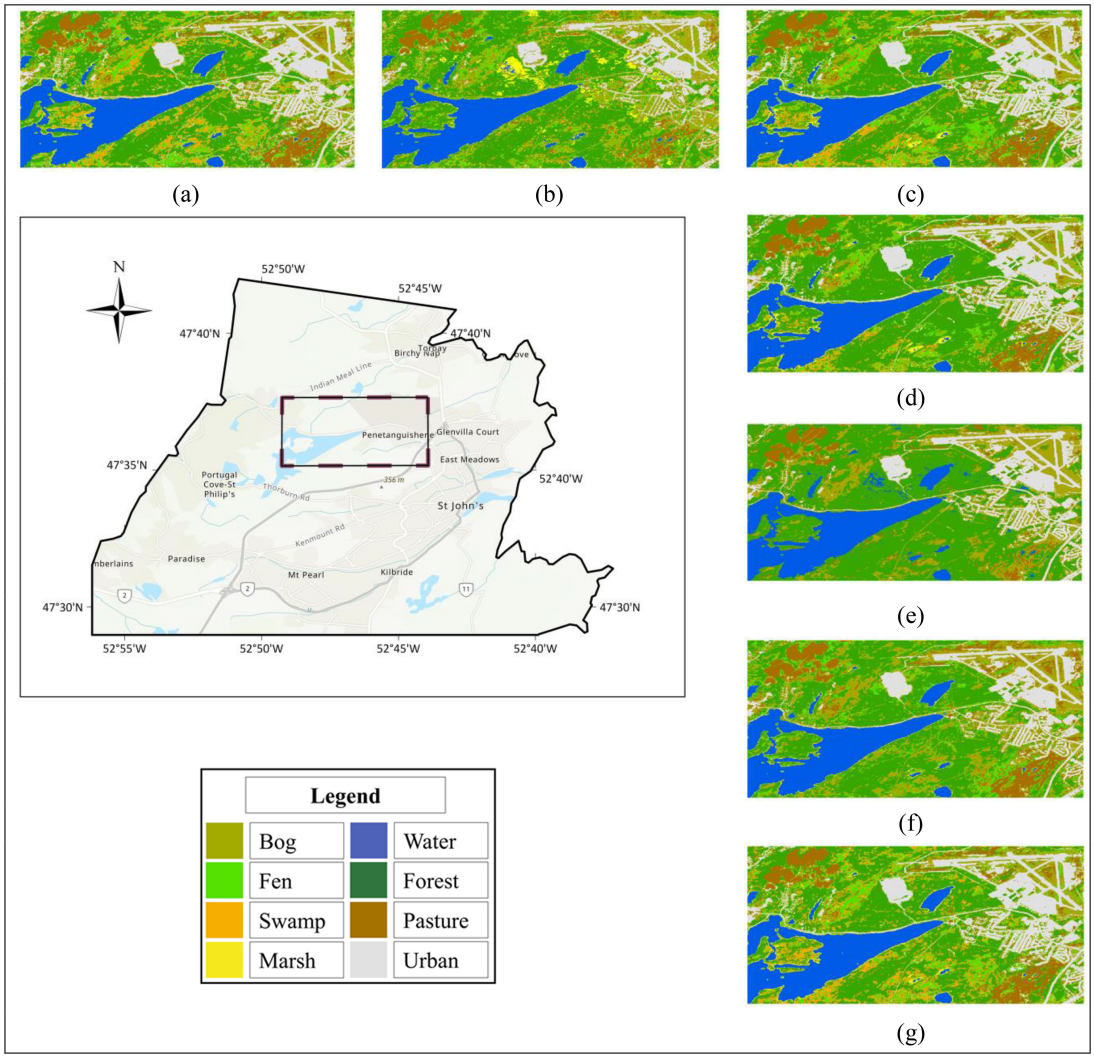

Fig. 5. Zoomed-in representation of a small portion of the classification maps obtained by (a) RF, (b) SVM, (c) XGB, (d) ResNet50, (e) GCN-branch, (f) CNN-branch, and (g) Wet-GC.

TABLE IX
ACCURACY ASSESSMENT INDICES OF EMPLOYED APPROACHES IN THIS ARTICLE

Methods	OA (%)	Recall	Specificity	Precision	F-score
RF	84.88	0.7180	0.9777	0.6987	0.7082
SVM	82.86	0.6922	0.9745	0.6713	0.6816
XGB	86.55	0.7181	0.9811	0.6887	0.7031
ResNet50	86.93	0.7154	0.9780	0.6919	0.7172
GCN-branch	77.70	0.5696	0.9609	0.5888	0.5790
CNN-branch	79.01	0.6174	0.9665	0.6122	0.6135
Wet-GC	88.68	0.7567	0.9838	0.7484	0.7525

Wet-GC method, and the lowest scores are produced by the SVM method. The differences between recall, specificity, precision, and F-score parameters for the proposed method (Wet-GC) and the maximum accuracy obtained for these parameters among the other methods (i.e., SVM, RF, XGB, and ResNet50) are about 0.039, 0.003, 0.05, and 0.035, respectively.

The conclusion about the performance of Wet-GC can also be drawn when comparing the confusion matrices. According to Fig. 6, wetland classes' classification has lower accuracy than nonwetland classes. Notably, all methods successfully classified over 87% of the nonwetland classes (i.e., water, forest, pasture, and urban). The Wet-GC model was the most successful

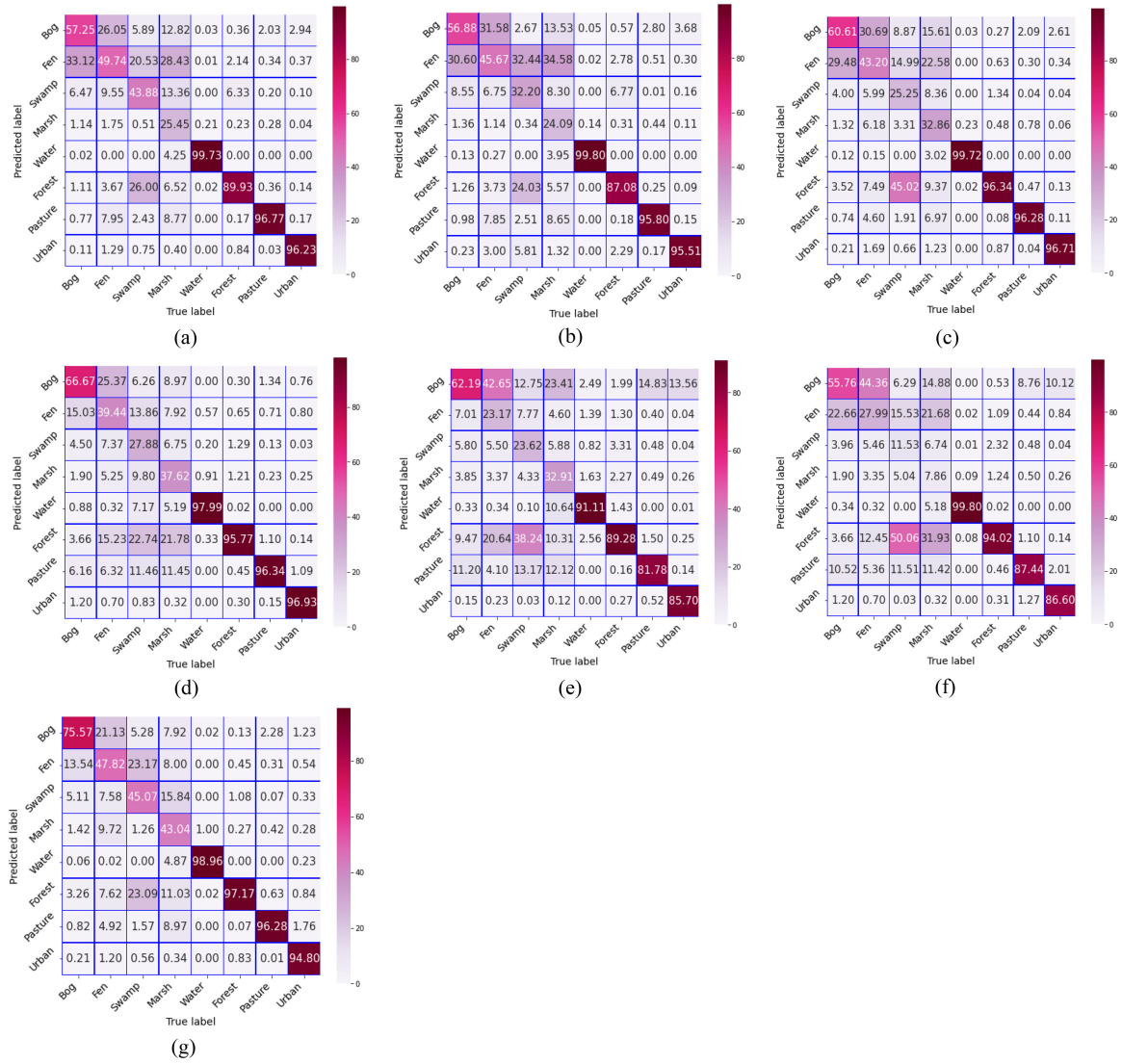

Fig. 6. Confusion matrices summarizing the accuracy of results based on the evaluation of different algorithms. (a) RF. (b) SVM. (c) XGB. (d) ResNet50. (e) GCN-branch. (f) CNN-branch. (g) Wet-GC. Each entry of the confusion matrices is shown as a percentage calculated from the total number of entries in each column.

TABLE X
APPROXIMATE EXECUTION TIME OF THE CLASSIFICATION MODELS

Methods	Processing time (minutes)
RF	8
SVM	13
XGB	11
ResNet50	77
GCN-branch	59
CNN-branch	42
Wet-GC	84

approach for classifying the nonwetland classes among all the methods. However, the wetland classes were also identified with high accuracies when Wet-GC was applied. In the case of other methods, some misclassifications in wetland classes look relatively impressive. For instance, about 33% of bog classes were misclassified as fen in the RF method, and more than 30% of fen classes were misclassified as bog in the SVM method. In addition, in the XGB and ResNet50 models, about 25% and 28% of swamp classes, respectively, were classified correctly.

In distinguishing wetland classes, the Wet-GC method was also the best one. More than 43% of fen, swamp, and marsh classes were correctly classified in Wet-GC, and beyond 75% of bog classes. The efficiency of Wet-GC could be due to CNNs' nature, which is to extract and add new features for training the network, combined with the GCNs' nature, which is to explore the spatial relations of the pixels (in fact, the wetland classes). Moreover, all the models use the S1 and S2 images as stacked data and apply the classification procedure for the data at once. In contrast, the Wet-GC method deals with each dataset separately and through two branches, which are inherently designed for such datasets. In particular, the CNN branch handles the contextual information in S2 multispectral data, while the mini-GCN

branch takes into account the spatial relationships of pixels in S1 data.

VI. Conclusion

Wetlands are one of the most unique, valuable, and beautiful ecosystem types on earth and perform a variety of ecological and socio-economic benefits. However, anthropogenic activities significantly threaten wetlands' capacity and their services. Hence, mapping these productive resources is crucial to monitor their status (changes and losses). RS-based approaches are time- and cost-effective solutions and superior to laborious fieldwork when dealing with large-scale wetland classification. Although several DL-based models in the literature have achieved outstanding wetland classification performance, some complex scene classes are still easily misclassified when only a limited number of training samples are available. Thus, exploring new models that require fewer training samples remains a necessity.

This article proposed a novel Wet-GC workflow, which jointly uses the GCN and CNN models. The proposed approach was examined using S1 and S2 imagery and revealed promising results for the classification of wetlands' scenes with minimal need for training samples. This article is the first one investigating the GCN model's performance for large-scale wetland classification using the combination of SAR and optical imagery. The experimental results demonstrate the superiority of the developed framework over the RF, SVM, XGB, and ResNet50 methods. For future work, incorporating richer multispectral data and additional SAR data features to improve the Wet-GC architecture's efficiency and increase the discriminability of the wetland categories is suggested. It is also recommended to employ the proposed method for provincial-scale wetland classification with a variety of training sample sizes. A new study could also be conducted to examine the impacts of different ratios of training samples for each class when GCNs are used.

Acknowledgment

The authors would like to thank European Space Agency for providing S1 and S2 open-access data and also like to sincere thanks anonymous reviewers for their valuable comments and constructive suggestions that helped improve the clarity of the manuscript. The authors are indebted to several organizations who collected field data, including Ducks Unlimited Canada, the Government of Newfoundland and Labrador Department of Environment and Conservation, and Nature Conservancy Canada.

References

[1] M. Guo, J. Li, C. Sheng, J. Xu, and L. Wu, "A review of wetland remote sensing," *Sensors*, vol. 17, no. 4, pp. 1–36, Apr. 2017, doi: 10.3390/s17040777.

[2] R. Tiner, *Wetland Indicators: A Guide to Wetland Formation, Identification, Delineation, Classification, and Mapping, Second Edition*. Boca Raton, FL, USA: CRC Press, 2016.

[3] M. Mahdianpari *et al.*, "A large-scale change monitoring of wetlands using time series Landsat imagery on Google Earth Engine: A case study in Newfoundland," *GIScience Remote Sens.*, vol. 57, no. 8, pp. 1102–1124, Nov. 2020, doi: 10.1080/15481603.2020.1846948.

[4] A. L. Gallant, "The challenges of remote monitoring of wetlands," *Remote Sens.*, vol. 7, no. 8, pp. 10938–10950, Aug. 2015, doi: 10.3390/rs70810938.

[5] G. Kaplan and U. Avdan, "Monthly analysis of wetlands dynamics using remote sensing data," *ISPRS Int. J. Geo-Inf.*, vol. 7, no. 10, p. 411, 2018.

[6] M. Mahdianpari *et al.*, "The second generation Canadian wetland inventory map at 10 meters resolution using Google Earth Engine," *Can. J. Remote Sens.*, vol. 46, no. 3, pp. 360–375, Aug. 2020, doi: 10.1080/07038992.2020.1802584.

[7] M. Mahdianpari *et al.*, "Monitoring of 30 years wetland changes in Newfoundland, Canada," in *Proc. IEEE Int. Geosci. Remote Sens. Symp.*, 2021, pp. 88–91, doi: 10.1109/IGARSS47720.2021.9553053.

[8] M. Mahdianpari *et al.*, "Big data for a big country: The first generation of Canadian wetland inventory map at a spatial resolution of 10-m using sentinel-1 and sentinel-2 data on the Google Earth Engine cloud computing platform," *Can. J. Remote Sens.*, vol. 46, no. 1, pp. 15–33, 2020.

[9] C. Fang, Z. Tao, D. Gao, and H. Wu, "Wetland mapping and wetland temporal dynamic analysis in the Nanjishan wetland using gaofen one data," *Ann. GIS*, vol. 22, no. 4, pp. 259–271, Oct. 2016, doi: 10.1080/19475683.2016.1231719.

[10] D. Were, F. Kansiime, T. Fetahi, A. Cooper, and C. Jjuuko, "Carbon sequestration by wetlands: A critical review of enhancement measures for climate change mitigation," *Earth Syst. Environ.*, vol. 3, no. 2, pp. 327–340, Aug. 2019, doi: 10.1007/s41748-019-00094-0.

[11] C. H. Marshall, R. A. Pielke, and L. T. Steyaert, "Has the conversion of natural wetlands to agricultural land increased the incidence and severity of damaging freezes in South Florida?," *Monthly Weather Rev.*, vol. 132, no. 9, pp. 2243–2258, Sep. 2004, doi: 10.1175/1520-0493.

[12] G. D. Lynne, P. Conroy, and F. J. Prochaska, "Economic valuation of marsh areas for marine production processes," *J. Environ. Econ. Manage.*, vol. 8, no. 2, pp. 175–186, Jun. 1981, doi: 10.1016/0095-0696(81)90006-1.

[13] C. N. Raphael and E. Jaworski, "Economic value of fish, wildlife, and recreation in Michigan's coastal wetlands," *Coastal Zone Manage. J.*, vol. 5, no. 3, pp. 181–194, Jan. 1979, doi: 10.1080/08920757909361805.

[14] R. Costanza, O. Pérez-Maqueo, M. L. Martinez, P. Sutton, S. J. Anderson, and K. Mulder, "The value of coastal wetlands for Hurricane protection," *Ambio*, vol. 37, no. 4, pp. 241–248, 2008.

[15] R. C. Gardner *et al.*, *State of the World's Wetlands and Their Services to People: A Compilation of Recent Analyses*. Gland, Switzerland: Ramsar Convention Secretariat, 2015.

[16] K. S. Schmidt and A. K. Skidmore, "Spectral discrimination of vegetation types in a coastal wetland," *Remote Sens. Environ.*, vol. 85, no. 1, pp. 92–108, Apr. 2003, doi: 10.1016/S0034-4257(02)00196-7.

[17] T. Landmann, M. Schramm, R. R. Colditz, A. Dietz, and S. Dech, "Wide area wetland mapping in semi-arid Africa using 250-meter MODIS metrics and topographic variables," *Remote Sens.*, vol. 2, no. 7, pp. 1751–1766, Jul. 2010, doi: 10.3390/rs2071751.

[18] S. C. Zoltai and D. H. Vitt, "Canadian wetlands: Environmental gradients and classification," *Vegetatio*, vol. 118, no. 1, pp. 131–137, Jun. 1995, doi: 10.1007/BF00045195.

[19] S. Mahdavi, B. Salehi, J. Granger, M. Amani, B. Brisco, and W. Huang, "Remote sensing for wetland classification: A comprehensive review," *GIScience Remote Sens.*, vol. 55, no. 5, pp. 623–658, Sep. 2018, doi: 10.1080/15481603.2017.1419602.

[20] F. M. Henderson and A. J. Lewis, "Radar detection of wetland ecosystems: A review," *Int. J. Remote Sens.*, vol. 29, no. 20, pp. 5809–5835, Oct. 2008, doi: 10.1080/01431160801958405.

[21] E. R. DeLancey, J. F. Simms, M. Mahdianpari, B. Brisco, C. Mahoney, and J. Kariyeva, "Comparing deep learning and shallow learning for large-scale wetland classification in Alberta, Canada," *Remote Sens.*, vol. 12, no. 1, pp. 1–20, Jan. 2020, doi: 10.3390/rs12010002.

[22] A. L. Gallant *et al.*, "Detecting emergence, growth, and senescence of wetland vegetation with polarimetric synthetic aperture radar (SAR) data," *Water*, vol. 6, no. 3, pp. 694–722, Mar. 2014, doi: 10.3390/w6030694.

[23] E. S. Kasischke, K. B. Smith, L. L. Bourgeau-Chavez, E. A. Romanowicz, S. Brunzell, and C. J. Richardson, "Effects of seasonal hydrologic patterns in south Florida wetlands on radar backscatter measured from ERS-2 SAR imagery," *Remote Sens. Environ.*, vol. 88, no. 4, pp. 423–441, Dec. 2003, doi: 10.1016/j.rse.2003.08.016.

[24] S. O. Mabwoga and A. K. Thukral, "Characterization of change in the Harike wetland, a Ramsar site in India, using landsat satellite data," *SpringerPlus*, vol. 3, no. 1, 2014, Art. no. 576.

[25] M. J. McCarthy, E. J. Merton, and F. E. Muller-Karger, "Improved coastal wetland mapping using very-high 2-meter spatial resolution imagery," *Int. J. Appl. Earth Observ. Geoinformation*, vol. 40, pp. 11–18, 2015.

[26] R. Shen, A. Huang, B. Li, and J. Guo, "Construction of a drought monitoring model using deep learning based on multi-source remote sensing data," *Int. J. Appl. Earth Observ. Geoinformation*, vol. 79, pp. 48–57, Jul. 2019, doi: 10.1016/j.jag.2019.03.006.

[27] H. Chen, C. Wu, B. Du, L. Zhang, and L. Wang, "Change detection in multisource VHR images via deep siamese convolutional multiple-layers recurrent neural network," *IEEE Trans. Geosci. Remote Sens.*, vol. 58, no. 4, pp. 2848–2864, Apr. 2020, doi: 10.1109/TGRS.2019.2956756.

[28] M. Li, P. Wu, B. Wang, H. Park, H. Yang, and Y. Wu, "A deep learning method of water body extraction from high resolution remote sensing images with multisensors," *IEEE J. Sel. Topics Appl. Earth Observ. Remote Sens.*, vol. 14, pp. 3120–3132, 2021, doi: 10.1109/JSTARS.2021.3060769.

[29] B. Hosseiny, M. Mahdianpari, B. Brisco, F. Mohammadimanesh, and B. Salehi, "WetNet: A spatial–temporal ensemble deep learning model for wetland classification using sentinel-1 and sentinel-2," *IEEE Trans. Geosci. Remote Sens.*, vol. 60, 2022, Art. no. 4406014, doi: 10.1109/TGRS.2021.3113856.

[30] D. Amarsaikhan, H. H. Blotevogel, J. L. van Genderen, M. Ganzorig, R. Gantuya, and B. Nergui, "Fusing high-resolution SAR and optical imagery for improved urban land cover study and classification," *Int. J. Image Data Fusion*, vol. 1, no. 1, pp. 83–97, Mar. 2010, doi: 10.1080/19479830903562041.

[31] S. van Beijma, A. Comber, and A. Lamb, "Random forest classification of salt marsh vegetation habitats using quad-polarimetric airborne SAR, elevation and optical RS data," *Remote Sens. Environ.*, vol. 149, pp. 118–129, Jun. 2014, doi: 10.1016/j.rse.2014.04.010.

[32] J. Zhang, "Multi-source remote sensing data fusion: Status and trends," *Int. J. Image Data Fusion*, vol. 1, no. 1, pp. 5–24, Mar. 2010, doi: 10.1080/19479830903561035.

[33] M. Mahdianpari, B. Salehi, F. Mohammadimanesh, S. Homayouni, and E. Gill, "The first wetland inventory map of Newfoundland at a spatial resolution of 10 m using sentinel-1 and sentinel-2 data on the Google Earth Engine cloud computing platform," *Remote Sens.*, vol. 11, no. 1, p. 43, Jan. 2019, doi: 10.3390/rs11010043.

[34] A. Jamali, M. Mahdianpari, B. Brisco, J. Granger, F. Mohammadimanesh, and B. Salehi, "Deep forest classifier for wetland mapping using the combination of sentinel-1 and sentinel-2 data," *GIScience Remote Sens.*, vol. 58, no. 7, pp. 1072–1089, Oct. 2021, doi: 10.1080/15481603.2021.1965399.

[35] M. Amani, B. Salehi, S. Mahdavi, and B. Brisco, "Spectral analysis of wetlands using multi-source optical satellite imagery," *ISPRS J. Photogrammetry Remote Sens.*, vol. 144, pp. 119–136, Oct. 2018, doi: 10.1016/j.isprsjprs.2018.07.005.

[36] E. Maggiori, Y. Tarabalka, G. Charpiat, and P. Alliez, "Convolutional neural networks for large-scale remote-sensing image classification," *IEEE Trans. Geosci. Remote Sens.*, vol. 55, no. 2, pp. 645–657, Feb. 2017, doi: 10.1109/TGRS.2016.2612821.

[37] W. Zhang, P. Tang, and L. Zhao, "Remote sensing image scene classification using CNN-CapsNet," *Remote Sens.*, vol. 11, no. 5, p. 494, Jan. 2019, doi: 10.3390/rs11050494.

[38] Q. Wang, Z. Yuan, Q. Du, and X. Li, "GETNET: A general end-to-end 2-D CNN framework for hyperspectral image change detection," *IEEE Trans. Geosci. Remote Sens.*, vol. 57, no. 1, pp. 3–13, Jan. 2019, doi: 10.1109/TGRS.2018.2849692.

[39] B. Yu, L. Yang, and F. Chen, "Semantic segmentation for high spatial resolution remote sensing images based on convolution neural network and pyramid pooling module," *IEEE J. Sel. Topics Appl. Earth Observ. Remote Sens.*, vol. 11, no. 9, pp. 3252–3261, Sep. 2018, doi: 10.1109/JSTARS.2018.2860989.

[40] G. Wang, B. Fan, S. Xiang, and C. Pan, "Aggregating rich hierarchical features for scene classification in remote sensing imagery," *IEEE J. Sel. Topics Appl. Earth Observ. Remote Sens.*, vol. 10, no. 9, pp. 4104–4115, Sep. 2017, doi: 10.1109/JSTARS.2017.2705419.

[41] X. Liu, Y. Zhou, J. Zhao, R. Yao, B. Liu, and Y. Zheng, "Siamese convolutional neural networks for remote sensing scene classification," *IEEE Geosci. Remote Sens. Lett.*, vol. 16, no. 8, pp. 1200–1204, Aug. 2019, doi: 10.1109/LGRS.2019.2894399.

[42] J. Xie, N. He, L. Fang, and A. Plaza, "Scale-free convolutional neural network for remote sensing scene classification," *IEEE Trans. Geosci. Remote Sens.*, vol. 57, no. 9, pp. 6916–6928, Sep. 2019, doi: 10.1109/TGRS.2019.2909695.

[43] M. Rezaee, M. Mahdianpari, Y. Zhang, and B. Salehi, "Deep convolutional neural network for complex wetland classification using optical remote sensing imagery," *IEEE J. Sel. Topics Appl. Earth Observ. Remote Sens.*, vol. 11, no. 9, pp. 3030–3039, Sep. 2018, doi: 10.1109/JSTARS.2018.2846178.

[44] G. L. O'Neil, J. L. Goodall, M. Behl, and L. Saby, "Deep learning using physically-informed input data for wetland identification," *Environ. Model. Softw.*, vol. 126, Apr. 2020, Art. no. 104665, doi: 10.1016/j.envsoft.2020.104665.

[45] A. Jamali and M. Mahdianpari, "Swin transformer and deep convolutional neural networks for coastal wetland classification using sentinel-1, sentinel-2, and LiDAR data," *Remote Sens.*, vol. 14, no. 2, p. 359, Jan. 2022, doi: 10.3390/rs14020359.

[46] Y. Gao, J. Shi, J. Li, and R. Wang, "Remote sensing scene classification based on high-order graph convolutional network," *Eur. J. Remote Sens.*, vol. 54, no. 1, pp. 141–155, Feb. 2021, doi: 10.1080/22797254.2020.1868273.

[47] B. Liu, K. Gao, A. Yu, W. Guo, R. Wang, and X. Zuo, "Semisupervised graph convolutional network for hyperspectral image classification," *JARS*, vol. 14, no. 2, Jun. 2020, Art. no. 026516, doi: 10.1117/1.JRS.14.026516.

[48] A. Sha, B. Wang, X. Wu, and L. Zhang, "Semisupervised classification for hyperspectral images using graph attention networks," *IEEE Geosci. Remote Sens. Lett.*, vol. 18, no. 1, pp. 157–161, Jan. 2021, doi: 10.1109/LGRS.2020.2966239.

[49] S. Wan, C. Gong, P. Zhong, S. Pan, G. Li, and J. Yang, "Hyperspectral image classification with context-aware dynamic graph convolutional network," *IEEE Trans. Geosci. Remote Sens.*, vol. 59, no. 1, pp. 597–612, Jan. 2021, doi: 10.1109/TGRS.2020.2994205.

[50] S. Wan, C. Gong, P. Zhong, B. Du, L. Zhang, and J. Yang, "Multiscale dynamic graph convolutional network for hyperspectral image classification," *IEEE Trans. Geosci. Remote Sens.*, vol. 58, no. 5, pp. 3162–3177, May 2020, doi: 10.1109/TGRS.2019.2949180.

[51] L. Mou, X. Lu, X. Li, and X. X. Zhu, "Nonlocal graph convolutional networks for hyperspectral image classification," *IEEE Trans. Geosci. Remote Sens.*, vol. 58, no. 12, pp. 8246–8257, Dec. 2020, doi: 10.1109/TGRS.2020.2973363.

[52] D. Hong, L. Gao, J. Yao, B. Zhang, A. Plaza, and J. Chanussot, "Graph convolutional networks for hyperspectral image classification," *IEEE Trans. Geosci. Remote Sens.*, vol. 59, no. 7, pp. 5966–5978, Jul. 2021, doi: 10.1109/TGRS.2020.3015157.

[53] V. Mazzia, A. Khaliq, and M. Chiaberge, "Improvement in land cover and crop classification based on temporal features learning from sentinel-2 data using recurrent-convolutional neural network (R-CNN)," *Appl. Sci.*, vol. 10, no. 1, p. 238, Jan. 2020, doi: 10.3390/app10010238.

[54] D. Ienco, R. Interdonato, R. Gaetano, and D. Ho Tong Minh, "Combining sentinel-1 and sentinel-2 satellite image time series for land cover mapping via a multi-source deep learning architecture," *ISPRS J. Photogrammetry Remote Sens.*, vol. 158, pp. 11–22, Dec. 2019, doi: 10.1016/j.isprsjprs.2019.09.016.

[55] M. Gori, G. Monfardini, and F. Scarselli, "A new model for learning in graph domains," in *Proc.. IEEE Int. Joint Conf. Neural Netw.*, 2005, vol. 2, pp. 729–734, doi: 10.1109/IJCNN.2005.1555942.

[56] D. Hong, N. Yokoya, N. Ge, J. Chanussot, and X. X. Zhu, "Learnable manifold alignment (LeMA): A semi-supervised cross-modality learning framework for land cover and land use classification," *ISPRS J. Photogrammetry Remote Sens.*, vol. 147, pp. 193–205, Jan. 2019, doi: 10.1016/j.isprsjprs.2018.10.006.

[57] C. D. McGillem and G. R. Cooper, *Continuous and Discrete Signal and System Analysis*. Oxford, U.K.: Oxford Univ. Press, 1991.

[58] K. He, X. Zhang, S. Ren, and J. Sun, "Spatial pyramid pooling in deep convolutional networks for visual recognition," *IEEE Trans. Pattern Anal. Mach. Intell.*, vol. 37, no. 9, pp. 1904–1916, Sep. 2015, doi: 10.1109/TPAMI.2015.2389824.

[59] H. Lee and H. Kwon, "Going deeper with contextual CNN for hyperspectral image classification," *IEEE Trans. Image Process.*, vol. 26, no. 10, pp. 4843–4855, Oct. 2017, doi: 10.1109/TIP.2017.2725580.

[60] M. Mahdianpari, B. Salehi, F. Mohammadimanesh, and M. Motagh, "Random forest wetland classification using ALOS-2 L-band, RADARSAT-2 C-band, and TerraSAR-X imagery," *ISPRS J. Photogrammetry Remote Sens.*, vol. 130, pp. 13–31, Aug. 2017, doi: 10.1016/j.isprsjprs.2017.05.010.

[61] N. Gorelick, M. Hancher, M. Dixon, S. Ilyushchenko, D. Thau, and R. Moore, "Google Earth Engine: Planetary-scale geospatial analysis for everyone," *Remote Sens. Environ.*, vol. 202, pp. 18–27, Dec. 2017, doi: 10.1016/j.rse.2017.06.031.

[62] K. Van Tricht, A. Gobin, S. Gilliams, and I. Piccard, "Synergistic use of radar sentinel-1 and optical sentinel-2 imagery for crop mapping: A case study for Belgium," *Remote Sens.*, vol. 10, no. 10, p. 1642, Oct. 2018, doi: 10.3390/rs10101642.

[63] B. Slagter, N.-E. Tsendbazar, A. Vollrath, and J. Reiche, "Mapping wetland characteristics using temporally dense sentinel-1 and sentinel-2 data: A case study in the St. Lucia wetlands, South Africa," *Int. J. Appl. Earth Observ. Geoinformation*, vol. 86, Apr. 2020, Art. no. 102009, doi: 10.1016/j.jag.2019.102009.

[64] K. He, X. Zhang, S. Ren, and J. Sun, "Deep residual learning for image recognition," 2016, pp. 770–778. Accessed: Apr. 19, 2022. [Online]. Available: https://openaccess.thecvf.com/content_cvpr_2016/html/He_Deep_Residual_Learning_CVPR_2016_paper.html

[65] H. Liu *et al.*, "Object-based multigrained cascade forest method for wetland classification using sentinel-2 and radarsat-2 imagery," *Water*, vol. 14, no. 1, p. 82, Jan. 2022, doi: 10.3390/w14010082.

[66] M. Mahdianpari, B. Salehi, M. Rezaee, F. Mohammadimanesh, and Y. Zhang, "Very deep convolutional neural networks for complex land cover mapping using multispectral remote sensing imagery," *Remote Sens.*, vol. 10, no. 7, p. 1119, Jul. 2018, doi: 10.3390/rs10071119.

[67] H. Jafarzadeh, M. Mahdianpari, E. Gill, F. Mohammadimanesh, and S. Homayouni, "Bagging and boosting ensemble classifiers for classification of multispectral, hyperspectral and PolSAR data: A comparative evaluation," *Remote Sens.*, vol. 13, no. 21, p. 4405, Jan. 2021, doi: 10.3390/rs13214405.

[68] H. Jafarzadeh and M. Hasanlou, "An unsupervised binary and multiple change detection approach for hyperspectral imagery based on spectral unmixing," *IEEE J. Sel. Topics Appl. Earth Observ. Remote Sens.*, vol. 12, no. 12, pp. 4888–4906, Dec. 2019, doi: 10.1109/JSTARS.2019.2939133.

Hamid Jafarzadeh (Student Member, IEEE) received the B.Sc. degree in surveying and geomatics engineering from the University of Tabriz, Tabriz, Iran, in 2016, and the M.Sc. degree in remote sensing engineering from the University of Tehran, Tehran, Iran, in 2020. He is currently working toward the Ph.D. degree in electrical engineering with the Department of Engineering and Applied Science, Memorial University, St. John's, NL, Canada.

His research interests include remote sensing and image processing, multispectral, hyperspectral, and SAR data analysis, machine learning, and multisensor data classification in environmental studies, with a special focus on wetland mapping and monitoring.

Masoud Mahdianpari (Senior Member, IEEE) received the B.S. degree in surveying and geomatics engineering and the M.Sc. degree in remote sensing engineering from the School of Surveying and Geomatics Engineering, College of Engineering, University of Tehran, Tehran, Iran, in 2010 and 2013, respectively, and the Ph.D. degree in electrical engineering from the Department of Engineering and Applied Science, Memorial University, St. John's, NL, Canada, in 2019.

In 2019, he was an Ocean Frontier Institute Postdoctoral Fellow with Memorial University and C-CORE. He is currently a Remote Sensing Technical Lead with C-CORE and a Cross Appointed Professor with the Faculty of Engineering and Applied Science, Memorial University. He has authored more than 100 publications, including peer-reviewed journal articles, conference papers, books, and book chapters. His research interests include remote sensing and image analysis, with a special focus on PolSAR image processing, multisensor data classification, machine learning, geo big data, and deep learning.

Dr. Mahdianpari is also an Editorial Team Member for the *Remote Sensing* journal and the *Canadian Journal of Remote Sensing*. He was a recipient of the Research and Development Corporation Ocean Industries Student Research Award, organized by Newfoundland Industry and Innovation Center, amongst more than 400 submissions, in 2016, the T. David Collett Best Industry Paper Award organized by IEEE in 2016, the Com-Adv Devices, Inc., Scholarship for Innovation, Creativity, and Entrepreneurship from the Memorial University in 2017, the Artificial Intelligence for Earth Grant organized by Microsoft in 2018, and the Graduate Academic Excellence Award organized by Memorial University in 2019. In 2020, he received the Best Industry Paper Award organized by IEEE Newfoundland Electrical and Computer Engineering Conference.

Eric W. Gill (Senior Member, IEEE) received the B.Sc. degree (hons.) in physics and the M.Eng. and Ph.D. degrees in electrical engineering from the Memorial University of Newfoundland, St. John's, NL, Canada, in 1977, 1990, and 1999, respectively.

In 1977, he was a Lecturer in physics with the College of the North Atlantic, St. John's. Since 2000, he has been with the Faculty of Engineering and Applied Science, Memorial University of Newfoundland, where he is currently a Professor Emeritus conducting research in theoretical and applied electromagnetics. Originally, his research interests include primarily associated with the scattering of high-frequency electromagnetic radiation from time-varying, randomly rough surfaces, with particular application to the use of surface wave radar in remote sensing of the ocean environment. In recent years, his interests have also included remote sensing using marine radar as well as scattering problems associated with sea ice and icebergs.

Dr. Gill, in addition to being the current Chair of the Newfoundland and Labrador Chapter of the IEEE Oceanic Engineering Society, also holds memberships of the IEEE Antennas and Propagation Society and the American Geophysical Union.